The hepatocyte insulin receptor is required to program the liver clock and rhythmic gene expression

Tiffany Fougeray, Arnaud Polizzi, Marion Régnier, Anne Fougerat, Sandrine Ellero-Simatos, Yannick Lippi, Sarra Smati, Frédéric Lasserre, Blandine Tramunt, Marine Huillet, et al.

HAL Id: hal-03647009
https://hal.inrae.fr/hal-03647009

Submitted on 20 Apr 2022

The hepatocyte insulin receptor is required to program the liver clock and rhythmic gene expression

Graphical abstract

Authors

Tiffany Fougeray, Arnaud Polizzi, Marion Régnier, ..., Catherine Postic, Alexandra Montagner, Hervé Guillou

Correspondence

alexandra.montagner@inserm.fr (A.M.), herve.guillou@inrae.fr (H.G.)

In brief

Gene expression is rhythmic and sensitive to various environmental and physiological stimuli. Food intake regulates insulin secretion, and feeding is a dominant signal for entraining the liver clock. Fougeray et al. show that an intact hepatocyte insulin receptor is required to program the liver clock and associated rhythmic gene expression.

Highlights

- Deletion of IR in hepatocytes induces a time-sensitive defect in glucose homeostasis

- IR deletion induces time-sensitive changes in liver gene expression

- IR deletion modifies liver circadian metabolic homeostasis and clock genes

- IR deletion alters programming of gene expression rhythmicity in response to feeding

CellPress

The hepatocyte insulin receptor is required to program the liver clock and rhythmic gene expression

Tiffany Fougeray,[1,2] Arnaud Polizzi,[1] Marion Régnier,[1] Anne Fougerat,[1] Sandrine Ellero-Simatos,[1] Yannick Lippi,[1] Sarra Smati,[1,2,3] Frédéric Lasserre,[1] Blandine Tramunt,[2,4] Marine Huillet,[1] Léonie Dopavogui,[1] Juliette Salvi,[5] Emmanuelle Nédélec,[5] Vincent Gigot,[5] Lorraine Smith,[1] Claire Naylies,[1] Caroline Sommer,[1] Joel T. Haas,[6] Walter Wahli,[1,7,8] Hélène Duez,[6] Pierre Gourdy,[2,4] Laurence Gamet-Payrastre,[1] Alexandre Benani,[5] Anne-Françoise Burnol,[9] Nicolas Loiseau,[1] Catherine Postic,[9] Alexandra Montagner,[2,10,*] and Hervé Guillou[1,10,11,*]

[1]Toxalim (Research Center in Food Toxicology), INRAE, ENVT, INP- PURPAN, UMR 1331, UPS, Université de Toulouse, 180 Chemin de Tournefeuille, 31027 Toulouse, France
[2]Institut des Maladies Métaboliques et Cardiovasculaires (I2MC), UMR1297, INSERM/UPS, Université de Toulouse, 1 Avenue Jean Poulhès, BP 84225, 31432 Toulouse, France
[3]Université de Nantes, INSERM, CNRS, CHU Nantes, Institut du Thorax, 44000 Nantes, France
[4]Service de Diabétologie, Maladies Métaboliques et Nutrition, CHU de Toulouse, Université de Toulouse, Toulouse, France
[5]Centre des Sciences du Goût et de l'Alimentation, CNRS, INRAE, Université Bourgogne Franche-Comté, Institut Agro Dijon, 21000 Dijon, France
[6]Univ. Lille, Inserm, CHU Lille, Institut Pasteur de Lille, U1011-EGID, F-59000 Lille, France
[7]Lee Kong Chian School of Medicine, Nanyang Technological University Singapore, Singapore 308232, Singapore
[8]Center for Integrative Genomics, University of Lausanne, Le Génopode, 1015 Lausanne, Switzerland
[9]Université de Paris, Institut Cochin, CNRS, INSERM, 75014 Paris, France
[10]These authors contributed equally
[11]Lead contact
*Correspondence: alexandra.montagner@inserm.fr (A.M.), herve.guillou@inrae.fr (H.G.)
https://doi.org/10.1016/j.celrep.2022.110674

SUMMARY

Liver physiology is circadian and sensitive to feeding and insulin. Food intake regulates insulin secretion and is a dominant signal for the liver clock. However, how much insulin contributes to the effect of feeding on the liver clock and rhythmic gene expression remains to be investigated. Insulin action partly depends on changes in insulin receptor (IR)-dependent gene expression. Here, we use hepatocyte-restricted gene deletion of IR to evaluate its role in the regulation and oscillation of gene expression as well as in the programming of the circadian clock in the adult mouse liver. We find that, in the absence of IR, the rhythmicity of core-clock gene expression is altered in response to day-restricted feeding. This change in core-clock gene expression is associated with defective reprogramming of liver gene expression. Our data show that an intact hepatocyte insulin receptor is required to program the liver clock and associated rhythmic gene expression.

INTRODUCTION

The mammalian clock system allows cells to anticipate environmental stimuli and synchronize daily physiological rhythms accordingly, which optimizes energy expenses (Bass and Takahashi, 2010; Green et al., 2008; Rijo-Ferreira and Takahashi, 2019; Guan and Lazar, 2021). The control of these oscillations involves transcriptional regulation by core-clock genes encoding the transcription factors CLOCK, BMAL1, PER1, PER2, CRY1, and CRY2 (Takahashi, 2017). At the organism level, the core-clock system of the suprachiasmatic nucleus of the hypothalamus is entrained by the light/dark cycle via retinal innervation and operates as the master regulator. It synchronizes peripheral clocks through various neuronal, physiological, and hormonal signals (Bass and Takahashi, 2010; Green et al., 2008; Mohawk et al., 2012). Moreover, food intake acts as a synchronizing cue for peripheral clocks such as the liver clock (Koronowski et al., 2019), which is particularly sensitive to feeding (Damiola et al., 2000; Droin et al., 2021; Greenwell et al., 2019; Saini et al., 2013; Stokkan et al., 2001; Vollmers et al., 2009; Weger et al., 2021, 2022). Similarly, insulin production by pancreatic β cells is clock controlled and responsive to feeding (Perelis et al., 2016). Therefore, circulating insulin may contribute to the resetting of peripheral clocks upon nutritional challenges.

Epidemiological studies have linked circadian disruption with metabolic diseases (Panda 2016; Perelis et al., 2016; Takahashi et al., 2008). Moreover, preclinical studies have shown that experimental diabetes and diet-induced obesity reprogram the liver clock (Kohsaka et al., 2007; Eckel-Mahan et al., 2013;

Guan et al., 2018; Panda 2016). Experiments performed in cell culture (Yamajuku et al., 2012) and *in vivo* (Sato et al., 2014) indicate that insulin can synchronize clock-gene expression in hepatocytes. Moreover, insulin and insulin-like growth factor-1 (IGF-1) regulate translation of PER clock proteins to entrain circadian rhythms with feeding *in vivo* (Crosby et al., 2019). Insulin and IGF-1 can signal through distinct pathways involving the insulin receptor (IR) (Batista et al., 2019a). IR activation can activate either AKT or Ras/MAP kinase signaling that ultimately influences the activity of several transcription factors involved in the control of hepatocyte growth and metabolism (Batista et al., 2019a), including activation of lipogenesis and inhibition of gluconeogenesis (Brown and Goldstein, 2008; Kubota et al., 2016; Li et al., 2010; Titchenell et al., 2017). Sterol regulatory element-binding transcription factor 1 (SREBP1c) is one such insulin-sensitive transcription factor and a potent regulator of lipogenesis in hepatocytes (Haas et al., 2012; Hegarty et al., 2005; Horton et al., 2002; Li et al., 2010). It also interacts with CRY1 to repress gluconeogenesis by promoting the degradation of forkhead box O1 (FOXO1) (Jang et al., 2016), a key transcription factor governing the expression of glucose-6-phosphatase (G6Pase) and phosphoenolpyruvate carboxykinase (PEPCK) (Dong et al., 2008; Matsumoto et al., 2007; O'Sullivan et al., 2015). IR can also directly translocate to the nucleus and form transcriptional complexes with RNA polymerase to control gene expression (Hancock et al., 2019).

In order to investigate the possible influence of IR on the liver clock *in vivo*, we used a mouse model of hepatocyte-restricted deletion of this receptor in hepatocytes, which are the main IR-expressing liver cell types (Michael et al., 2000) and have been shown to control liver chronophysiology in response to feeding (Guan et al., 2020).

RESULTS AND DISCUSSION

Hepatocyte-restricted deletion of IR induces a time-sensitive defect in glucose homeostasis

We verified the specificity of IR deletion in hepatocytes in adult mice (Figures 1A–1C) carrying LoxP sites flanking the fourth exon of the IR gene and expressing Cre recombinase in the liver under the control of the tamoxifen-inducible transthyretin promoter (IR$^{hep-/-}$) (Nemazanyy et al., 2015; Smati et al., 2020). Hepatocyte-restricted deletion of IR led to severe glucose intolerance (Figures 1D and 1E) combined with hyperinsulinemia (Figure 1F), likely due to both increased insulin secretion and decreased insulin clearance, as observed in mice with constitutive deletion of the receptor (Michael et al., 2000). Moreover, hepatocyte-restricted deletion of IR also led to decreased relative liver weight (Figure S1A) and reduced circulating high-density lipoprotein (HDL) cholesterol levels (Figure S1B), which recapitulate some key phenotypic traits of mice constitutively lacking IR in hepatocytes (Biddinger et al., 2008; Michael et al., 2000). Both insulinemia and glycemia were measured during the day (zeitgeber time [ZT]8) and during the night (ZT16), revealing increased hyperinsulinemia at day and night (Figure 1F), as well as hyperglycemia at night (Figure 1G), in animals fed *ad libitum*. At these two time points, we also measured a differential effect of IR loss in hepatocytes on additional

circulating lipids and hepatic metabolites (Figures S2A and S2B). Several reports have evidenced rhythmic phosphorylation of AKT in the liver of mice fed *ad libitum* (Jouffe et al., 2013; Vollmers et al., 2009). Our analyses are in agreement with these data and show that such rhythmicity depends on the expression of IR in hepatocytes (Figures 1H and 1I). We also confirm that AKT phosphorylation in the liver depends on IR expression in hepatocytes (Haas et al., 2012).

Hepatocyte-restricted deletion of IR induces time-sensitive changes in liver gene expression

To assess the contribution of IR to the control of nocturnal and diurnal liver activity, we analyzed liver gene expression during the day (ZT8) and at night (ZT16). Gene expression of enzymes acting in known insulin-sensitive pathways such as glycolysis, gluconeogenesis, and lipogenesis was altered by IR deletion (Figure 2A and S2C).

Genome-wide expression profiles revealed a set of genes (3,630) differentially expressed between IR$^{hep+/+}$ and IR$^{hep-/-}$ mice at both ZT8 and ZT16 (Figures 2B, S2D, and S2E; Table S1). Conversely, 1,907 genes were sensitive to timing (ZT8 versus ZT16) with little influence of IR deletion (Figure 2B). Finally, the largest group of genes (5,622) was both sensitive to timing and IR deletion (Figure 2B), suggesting an interaction between time and sensitivity to IR-dependent regulations.

To investigate these data further, we performed hierarchical clustering on these 11,159 differentially expressed genes and identified 10 broad patterns of gene expression (Figure 2C). The relative abundance of insulin-sensitive genes was measured in each cluster (Figure 2D), as determined by liver gene expression profiling following treatment with a physiological level of insulin (Batista et al., 2019b).

Clusters 3, 4, and 7 were sensitive to IR deletion but not to physiological insulin. This is likely due to ligand-independent IR activity, interference of IR deletion with IGF-1 signaling (Boucher et al., 2010; Nagao et al., 2021), and/or compensation of IR deletion. While we used a tamoxifen-induced IR deletion in adult mice to minimize such a risk, it is possible that some of the genes sensitive to IR deletion, but not to insulin, might also relate to the progressive hepatic dysfunction that has been reported in mice with liver-specific IR deletion (Michael et al., 2000).

Cluster 5 contains genes whose expression level is increased in the absence of IR (Figure 2C) and inhibited by physiological insulin treatment (Figure 2D), suggesting direct repression of gene expression engaging IR-dependent signaling. In line, we identified *Foxo1* target genes (Figure 2E) and genes involved in carbohydrate homeostasis (Figures 2E and S3A) as highly represented in this cluster. FOXO1 activity is known to regulate neoglucogenic enzymes and to be inhibited by insulin.

Clusters 1 and 2 contain genes whose expression is not sensitive to IR deletion but is inhibited by insulin (Figures 2E and S3A). Cluster 6 contains genes whose expression is not sensitive to IR deletion but is increased by physiological insulin (Figures 2E and S3A). All of these insulin-sensitive and IR-independent changes in gene expression likely reflect extra-hepatic insulin action on the control of hepatic functions (Titchenell et al., 2017).

Clusters 8, 9, and 10 contain genes whose expression level is decreased in the absence of IR (Figure 2C) and induced by
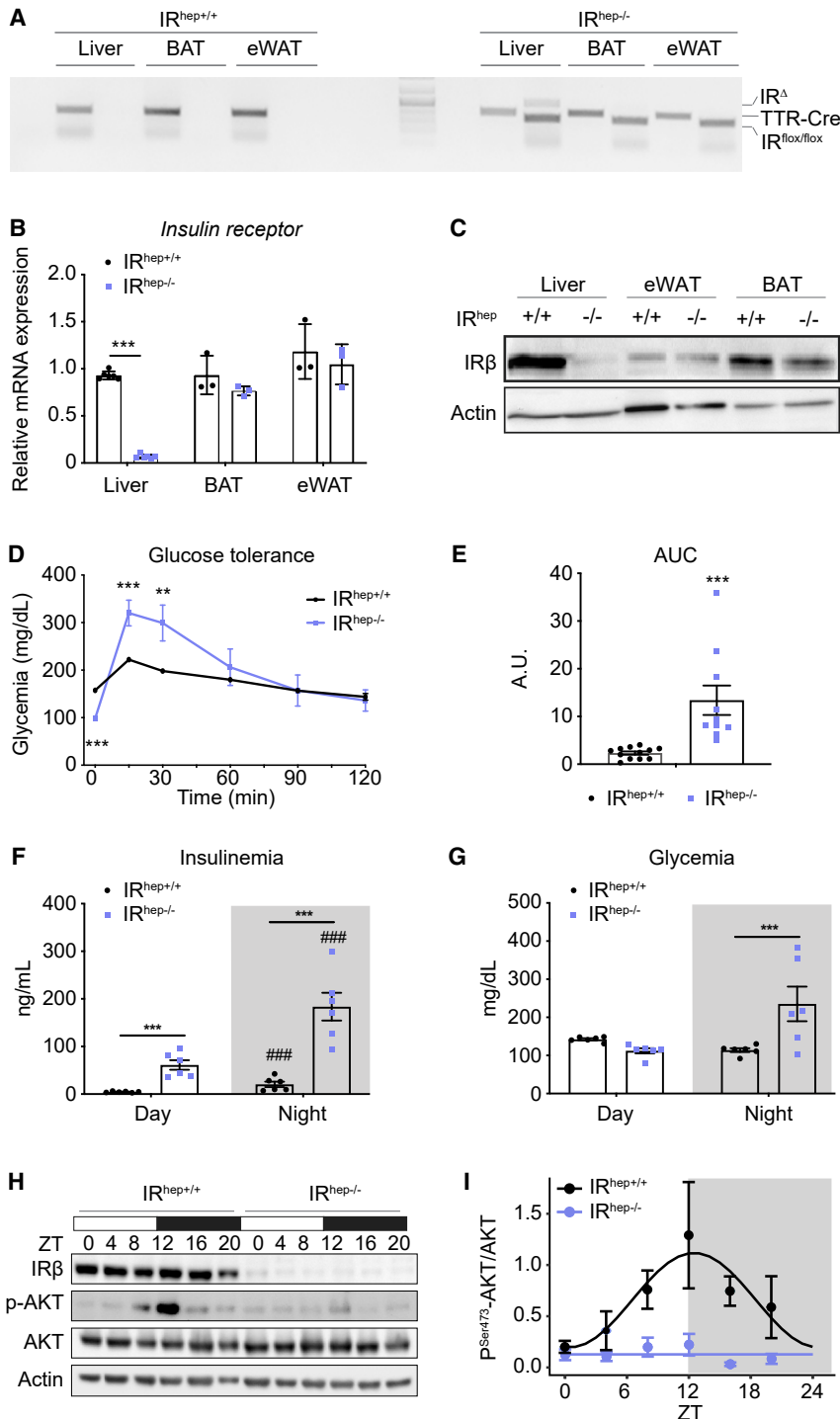
Figure 1. Hepatocyte-restricted deletion of the insulin receptor in adult mice leads to defective glucose homeostasis associated with impaired liver AKT signaling

(A) PCR analysis of insulin receptor (IR) floxed (IR[hep+/+]) and TTR-Tam-Cre (TTR-Tam-Cre^{+/−}) genes from mice that are liver wild type (WT) (IR[hep+/+]) or liver knockout (IR[hep−/−]) for IR using DNA extracted from different organs (n = 3 mice per group).

(B) Relative mRNA expression levels of IR from liver, epididymal white adipose tissue (eWAT), and brown adipose tissue (BAT) samples from IR[hep+/+] and IR[hep−/−] mice (n = 3 per group). Data represent mean ± SEM; statistical analysis was performed using two-way ANOVA with Sidak's multiple comparison test. *p < 0.05; **p < 0.01; ***p < 0.001.

(C) IR-β was assessed by western blotting in liver, eWAT, and BAT (blots are representative of three independent experiments).

(D and E) Glucose (2 g/kg) tolerance test after 6 h of fasting (D) and area under the curve (AUC) corresponding to the glucose tolerance test (E) (n = 10 mice per group). Data represent mean ± SEM; statistical significance was calculated using a two-tailed Student t-test with Bonferroni's multiple comparisons.

(F) Quantification of circulating insulin levels by ELISA (n = 6 per group). Data represent mean ± SEM; statistical analysis was performed using two-way ANOVA with Sidak's multiple comparison test. #, significant time effect; *, significant genotype effect. **p < 0.01; ***p < 0.001.

(G) Quantification of circulating glucose levels (n = 6 per group).

(H and I) IR-β, AKT phosphorylation, and total AKT were assessed around the clock by western blotting in liver of *ad libitum*-fed mice (H) and relative quantification of AKT phosphorylation over total AKT.

(I) Blots are representative of 5 independent experiments. Data represent mean ± SEM. Statistical analysis was performed using dryR algorithm. A flat line corresponds to no rhythm detected.

insulin's effect on lipogenesis (Haas et al., 2012; Hegarty et al., 2005; Horton et al., 2002; Li et al., 2010). We also identified significant enrichment in CLOCK and BMAL1 targets in cluster 10, suggesting a direct effect of insulin. Genes involved in this cluster are associated with metabolic homeostasis, which is consistent with the post-translational regulation of BMAL1 by insulin (Dang et al., 2016) and the established roles of CLOCK and BMAL1 in the control of metabolic func-

physiological insulin (Figure 2D), suggesting a direct and positive regulation engaging IR-dependent signaling. In line with this possibility, we identified SREBP1 target genes in cluster 8 (Figure 2D) enriched in genes involved in fatty acid and triglyceride synthesis (Figures 2E and S3A). This is consistent with the well-established role of SREBP1c as a mediator of

tions (Guan and Lazar, 2021). Finally, we found that among core-clock genes, *Per2*, which is regulated by the CLOCK:BMAL1 protein complex (Guan and Lazar, 2021) and is insulin sensitive (Batista et al., 2019b; Kuriyama et al., 2004; Yamajuku et al., 2012; Sato et al., 2014), is sensitive to IR deletion in hepatocytes (Figure S3B).
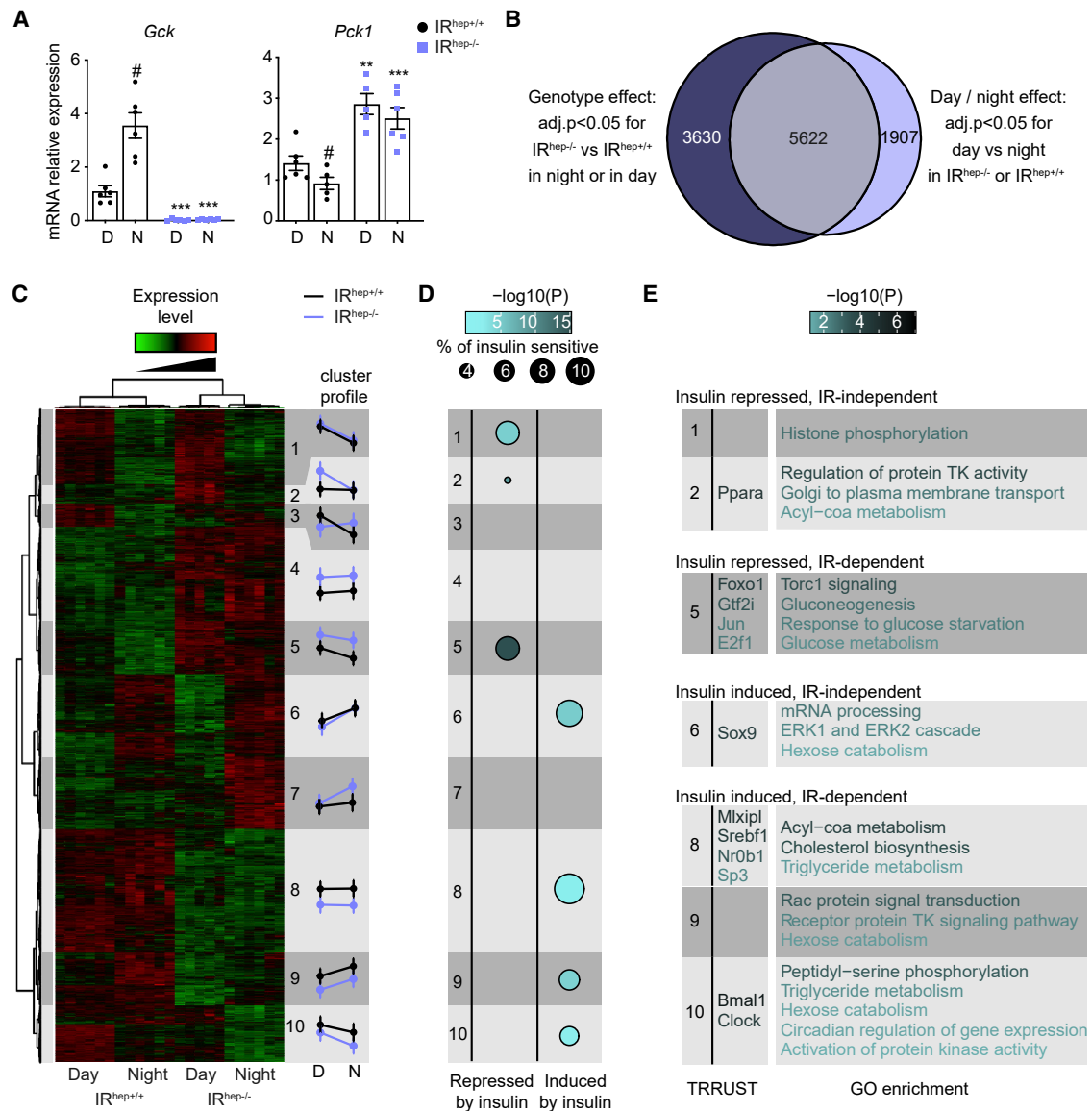
Figure 2. Hepatocyte-restricted deletion of the IR in adult mice induces time-sensitive changes in liver gene expression

Twelve-week-old IR[hep+/+] and IR[hep−/−] male mice were fed *ad libitum* and killed at ZT8 (day [D]) or ZT16 (night [N]).

(A) Relative mRNA expression levels of *Gck* and *Pck1* in liver samples (n = 5–6 per group). Data represent mean ± SEM; statistical analysis was performed using two-way ANOVA with Sidak's multiple comparisons test. # and *, significant effect of time and genotype, respectively. #, *p < 0.05; ##,**p < 0.01; ###,***p < 0.001.

(B) Euler diagram of the genes presenting a significant difference of expression for the genotype effect at night or at day, and the genes presenting a significant difference between night and day in IR[hep−/−] or IR[hep+/+].

(C) Heatmap based on expression level of 11,159 differentially expressed genes (n = 6 mice per group, individual values are represented). The schematic representation of the mean clusters profiles is plotted at the right of the heatmap.

(D) Enrichment in insulin-sensitive genes as determined by Batista et al. (2019b). The size of the circles is relative to the percentage of all identified insulin-sensitive genes within a cluster and the color to the p value of the hypergeometric test.

(E) Enrichment of transcription factors based on the TRRUST database (Han et al., 2018) and over Gene Ontology (GO) Biological Process (Pagès et al., 2021) are presented for clusters showing a significant enrichment in insulin-sensitive genes in (D). TRRUST enrichment over the whole transcriptome, and GO enrichment is performed over insulin-sensitive genes highlighted in (D) only. The gradient color of the characters strings is relative to the p value of the enrichment.

Effect of hepatocyte IR on circadian metabolic homeostasis and core-clock and clock-controlled genes in *ad libitum* feeding and in daytime-restricted feeding

Daytime-restricted feeding (DRF) uncouples the liver clock from the central clock (Damiola et al., 2000). We used DRF to challenge the liver clock and further investigate the role of hepatocyte IR in its programming. For this, 2 weeks post-induction of IR deletion, IR[hep−/−] and IR[hep+/+] control mice were fed *ad libitum* (AdLib) (Figure 3A) or fed only during the light phase (ZT0–ZT12) for 15 days (Figure 3B).
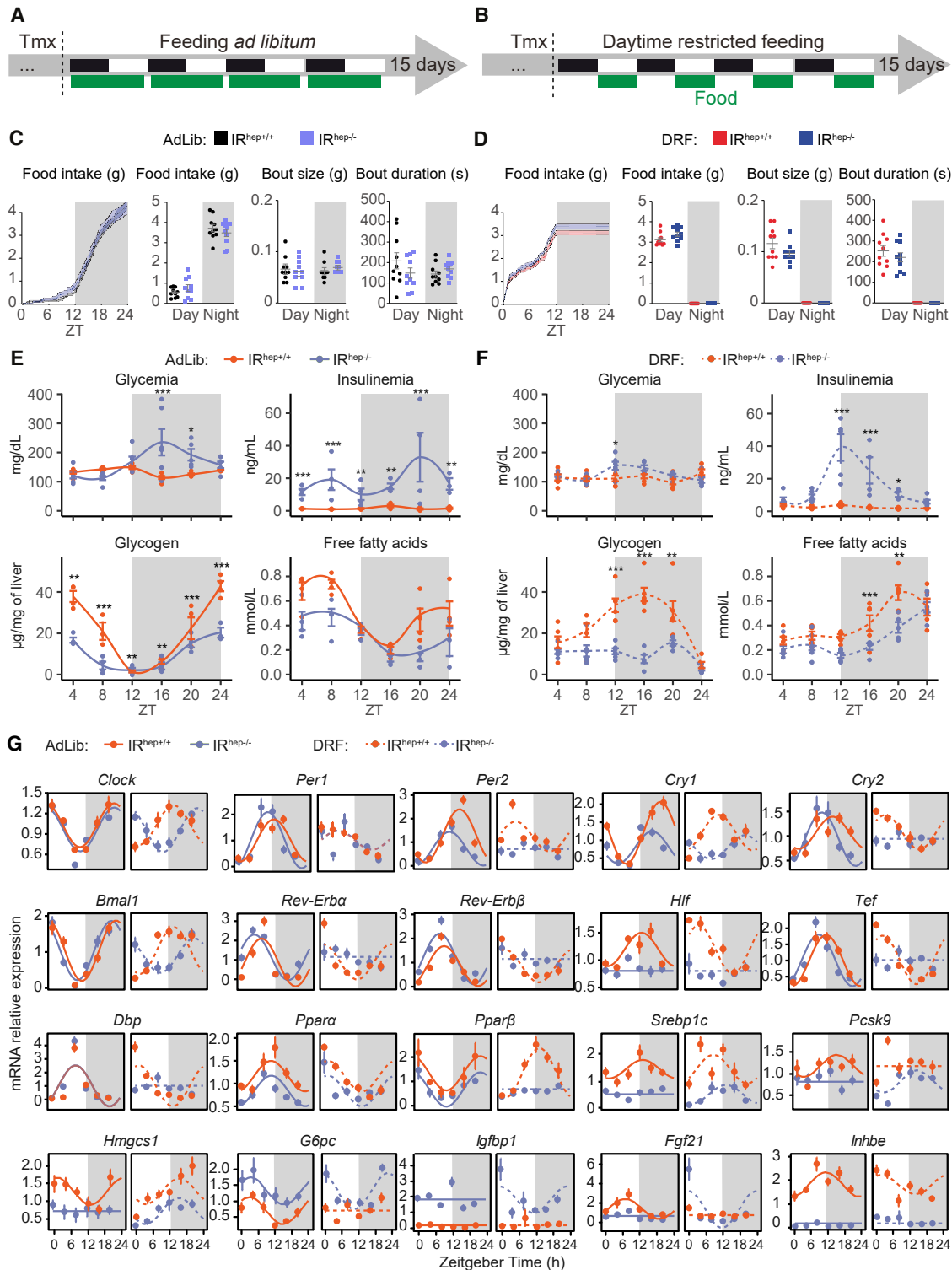
Figure 3. Hepatocyte-restricted deletion of the IR in adult mice influences circadian metabolic homeostasis and the expression of core-clock and clock-controlled genes *ad libitum* and upon daytime-restricted feeding (DRF)

Twelve-week-old IR[hep+/+] and IR[hep−/−] male mice (n = 10 per group) were fed either *ad libitum* (A) or upon DRF (B). Real-time food intake, average daily food intake, size, and duration of feeding bouts in mice fed *ad libitum* (C) and upon DRF (D).

(E) Quantification of circulating glucose, insulin, hepatic glycogen, and FFA levels (n = 6 mice per group) in mice fed *ad libitum*.

In both conditions, the rhythmicity of food intake was assessed (Figures 3C and 3D). IR[hep−/−] mice did not show a significant change in feeding rhythmicity, total food intake, or size and duration of feeding bouts compared with IR[hep+/+] mice when either fed AdLib or upon DRF.

Next, we examined the influence of AdLib and DRF on metabolic homeostasis. Hepatocyte-restricted deletion of IR induced a time-sensitive increase in glycemia, which was maximal at the beginning of the dark phase (Figure 3E), while in mice subjected to restricted feeding, it was maximal at ZT12 (Figure 3F). IR deletion induced hyperinsulinemia. In AdLib feeding, insulinemia was consistently higher in IR[hep−/−] mice than in IR[hep+/+] mice (Figure 3E). Upon DRF, hyperinsulinemia in IR[hep−/−] mice was maximal at the end of the light phase (ZT12) (Figure 3F), likely due to the change in feeding rhythm (Figure 3D). Hepatic glycogen content was consistently higher in IR[hep+/+] mice than in IR[hep−/−] mice upon AdLib feeding (Figure 3E), while such difference was only observed at night upon DRF (Figure 3F). Finally, free fatty acid (FFA) levels were higher during the light phase in AdLib-fed mice, with no significant difference between IR[hep+/+] and IR[hep−/−] mice (Figure 3E). In contrast, FFA levels were higher during the dark phase in mice of both genotypes upon DRF, which likely reflects adipose tissue lipolysis during the night (Figure 3F). Moreover, FFA levels in DRF mice during the dark phase were significantly increased in IR[hep+/+] mice when compared with IR[hep−/−] mice. Altogether, the impact of hepatocyte IR deletion on these metabolic markers was modified in AdLib feeding versus DRF.

We next examined the hepatic expression of core-clock genes as well as clock-controlled genes in IR[hep+/+] and IR[hep−/−] mice. Upon AdLib feeding, hepatocyte-restricted deletion of IR did not modify *Clock* expression but led to significant shifts in the rhythmic expression of some of the core-clock genes such as *Per2*, *Cry1*, and *Cry2* as well as clock-controlled genes such as *Hlf*, *Tef*, *Dbp*, *Pparα*, *Pparβ*, and *Tef* (Figure 3G, left panels). The expression of core-clock genes and clock-controlled genes was modified under restricted feeding and peaked with a 10–12 h shift when compared with their AdLib peaks (Figure 3G, right panels). Such IR-sensitive changes in the expression of core-clock genes were not observed in other insulin-sensitive tissues (Figure S4). Mice with hepatocyte-restricted IR deletion were not only refractory to DRF-mediated adaptation of the core-clock gene expression in the liver but also suggested differences in the relative expression of hepatic genes involved in lipid (*Srebp1c*, *Pcsk9*, *Hmgcs1*) and glucose (*G6pc*) homeostasis as well as hepatokines that coordinate systemic metabolic responses (*Igfbp1*, *Fgf21*, *Inhbe*).

Hepatocyte IR is required for the reprogramming of liver gene expression rhythmicity in response to DRF

Next, in order to further examine the potential consequences of such changes in the expression of core-clock genes, we performed a genome-wide analysis of the transcriptome IR[hep+/+] mice and IR[hep−/−] mice fed AdLib or submitted to DRF

(Table S2). To analyze differential rhythmicity across such multiple conditions, we used the recently published Differential Rhythmicity Analysis in R (dryR) package (Weger et al., 2021). This analysis first evidenced that DRF tends to reduce the number of rhythmic genes and the rhythmicity of their amplitude both in IR[hep+/+] and IR[hep−/−] mice when compared with AdLib feeding (Figure 4A). Moreover, we found that the difference in rhythmic gene expression between IR[hep+/+] and IR[hep−/−] mice is increased in DRF when compared with AdLib feeding (Figure 4B). In addition, we observed different shift profiles in DRF-induced shifts in rhythmic gene expression in IR[hep+/+] and IR[hep−/−] mice (Figure 4C).

We searched for rhythmic genes (AdLib) that would be reprogrammed by DRF and also for genes that may become rhythmic upon deletion of IR. Therefore, we identified 7 gene clusters that are either rhythmic in IR[hep+/+] or IR[hep−/−] mice or both AdLib and that have a different phase parameter either in IR[hep+/+] or IR[hep−/−] mice or in both upon DRF (Figures 4D and 4E).

Cluster 1 is IR independent and it includes 949 rhythmic genes independent of IR, as they were rhythmic in both IR[hep+/+] and IR[hep−/−] mice fed AdLib and similarly reprogrammed by DRF (Figure 4E).

Clusters 2 and 3 are clusters with IR-dependent gain of rhythmicity (Figure 4E). Cluster 2 includes 427 genes rhythmic in the liver only in the absence of hepatocyte IR. They are rhythmic in AdLib-fed IR[hep−/−] mice but not AdLib-fed IR[hep+/+] mice. These genes are also rhythmic in IR[hep−/−] mice upon DRF but not in IR[hep+/+] mice. Cluster 3 includes 609 genes that are rhythmic in both IR[hep+/+] and IR[hep−/−] mice fed AdLib that are only rhythmic in IR[hep−/−] mice upon DRF (Figure 4E).

Clusters 4, 5, 6, and 7 are IR sensitive. They include genes rhythmic in IR[hep+/+] mice fed AdLib and reprogrammed upon DRF in IR[hep+/+] mice. Cluster 4 contains 103 genes that are not rhythmic in the absence of IR either in AdLib-fed mice or upon DRF. Clusters 5 (123 genes), 6 (441 genes), and 7 (94) are rhythmic in the absence of IR in AdLib-fed mice. However, genes in cluster 5 show shifted rhythmicity in response to DRF in IR[hep−/−] mice when compared with IR[hep+/+] mice, genes in cluster 6 are not rhythmic in IR[hep−/−] mice, and genes in cluster 7 are not reprogrammed in response to DRF IR[hep−/−] mice.

To investigate the relevance of these 7 clusters of genes, we compared them with previously published data (Figure 4F). First, we analyzed the distribution of genes with hepatic expression driven by food intake in mice (Greenwell et al., 2019). Food-sensitive genes in IR-independent rhythmic cluster 1 and in clusters (4 and 6) were related to an IR-driven shift in rhythmicity induced by DRF. We also searched for genes with hepatic expression altered in mice with defective clock due to global deletion of *Bmal1*, one of the core-clock genes (Atger et al., 2015). This revealed numerous BMAL1-sensitive genes in IR-independent cluster 1 and in clusters 5, 6, and 7 related to genes depending on hepatocyte IR for change in rhythmicity induced by DRF.

(F) Quantification of circulating glucose, insulin, hepatic glycogen, and FFA levels (n = 6 mice per group) in mice upon DRF. Data represent mean ± SEM; statistical significance was calculated using two-way ANOVA with Sidak's multiple comparisons, *p < 0.05; **p < 0.01; ***p < 0.001.
(G) Relative mRNA expression levels of core-clock genes and clock-controlled genes (n = 6 per group). Data were analyzed with drylm function from the dryR package. Groups sharing the same fitting line shape have the same rhythmic parameters. A flat line signifies no rhythm detected.
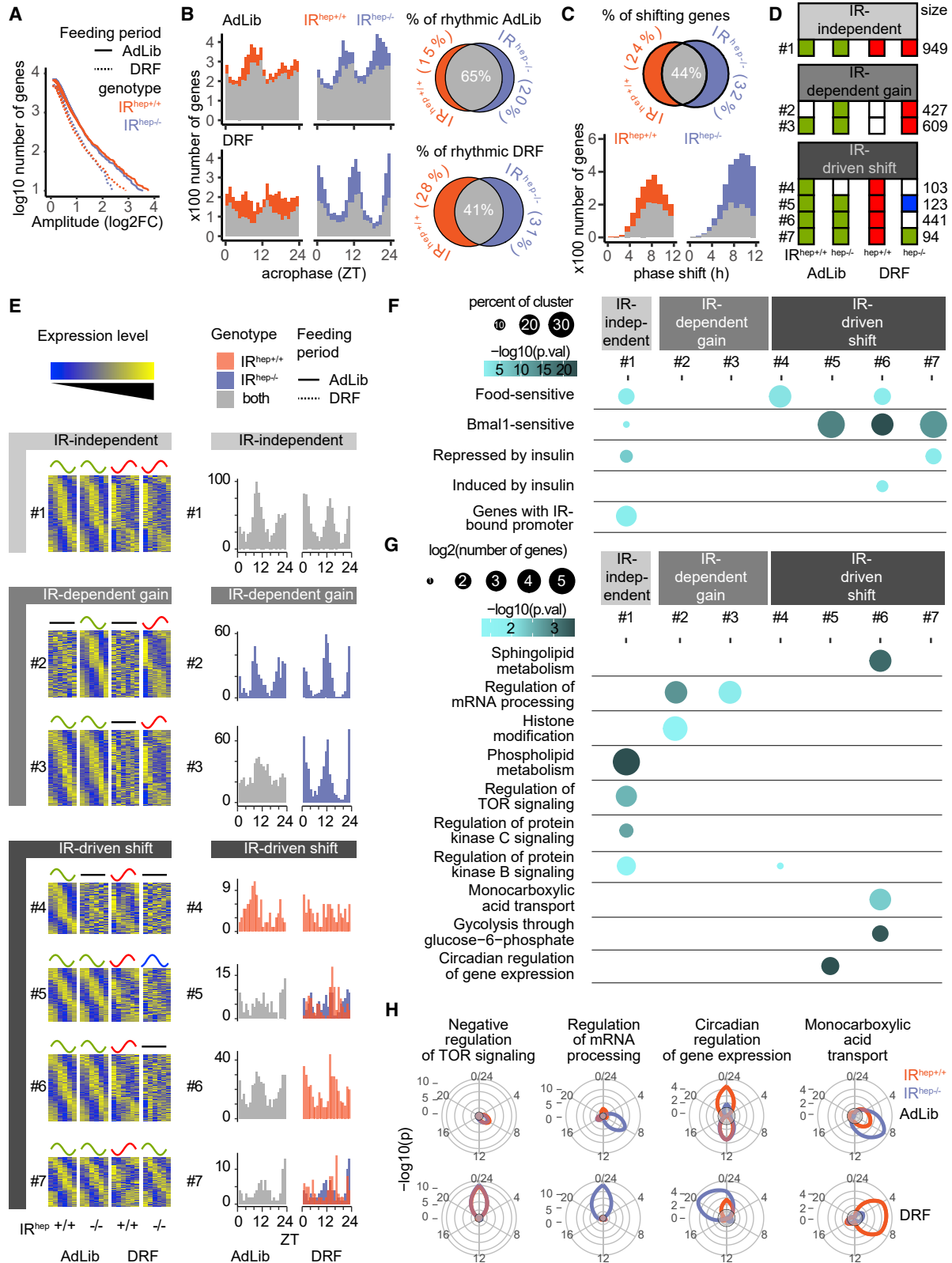
(legend on next page)

Hepatic genes affected by physiological insulin treatment *in vivo* in mouse (Batista et al., 2019b) were present in IR-independent cluster 1, suggesting indirect regulatory effects of insulin. They were also present in clusters 5, 6, and 7, related to IR-dependent changes in rhythmicity upon DRF. Finally, we also searched for the presence of genes with IR-bound promoters reported in human cells (Hancock et al.,2019), which were only enriched in IR-independent cluster 1.

Finally, we investigated the functional categories related to the genes in these clusters (Figures 4G and 4H). IR-independent cluster 1 is enriched in genes related to phospholipid metabolism as well as cell signaling through TOR, AKT/PKB, and PKC. The IR-dependent gains of rhythmicity related to clusters 2 and 3 were related to mRNA processing and histone modifications. Finally, IR-driven shifts in clusters 4, 5, 6, and 7 were related to metabolism, AKT/PKB signaling, and circadian regulation of gene expression. Altogether, these data show that intact hepatocyte IR is required for part of rhythmic gene expression in the liver.

Conclusions

Our work extends previous findings regarding the role of IR in the control of liver gene expression (Batista et al., 2019a, 2019b; Haas et al., 2012; Titchenell et al., 2017) and provides *in vivo* evidence that IR-dependent signaling in hepatocytes influences the liver clock. The loss of IR in hepatocytes led to both the shift or loss of pre-existing oscillations and a newly enhanced rhythmicity, which are typically observed after genetic manipulation of the liver core-clock genes and in diet-induced reprogramming of liver gene expression (Kohsaka et al., 2007; Eckel-Mahan et al., 2013; Guan et al., 2018; Panda, 2016).

We did not observe such defective rhythmicity and reprogramming of core-clock genes in other insulin-sensitive tissues, suggesting direct and cell-autonomous effects of IR deletion. There are three mechanisms by which IR influences gene expression in response to insulin: direct translocation to the nucleus and activation of either AKT-dependent or Ras/MAP-kinase-dependent signaling (Batista et al., 2019a, 2019b). Our analysis suggests it is unlikely to involve translocation of IR to the nucleus since genes with IR-bound promoters (Hancock et al., 2019) are not significantly enriched in clusters of genes

with IR-dependent changes in circadian expression. Which pathway downstream of IR is involved remains to be determined *in vivo*. In liver explants, PI3K inhibition has been shown to alter insulin-induced shifts of the *Per2*-driven reporter (Sato et al., 2014), and in H4IIe cells, PI3K inhibition blunts the induction of *Per2* expression by insulin (Yamajuku et al., 2012). The present work shows that *Per2* mRNA is sensitive to IR deletion in hepatocytes, that *Per2* rhythmicity is altered in the absence of IR, and that *Per2* expression cannot be reprogrammed in response to time-restricted feeding. These observations are in agreement with a direct effect of insulin on *Per2* expression (Batista et al., 2019b; Kuriyama et al., 2004; Yamajuku et al., 2012; Sato et al., 2014). We also show that the lack of hepatocyte IR influences the well-known rhythmicity of AKT phosphorylation *in vivo* (Aviram et al., 2021; Jouffe et al., 2013; Vollmers et al., 2009), which controls insulin-sensitive post-transcriptional regulation of BMAL1 (Dang et al., 2016). Further research is needed to investigate such a possible link between insulin, IR-mediated signaling through PI3K-AKT, core-clock gene activity, and their significance in metabolic homeostasis.

Moreover, our study highlights the effect of hepatocyte IR deletion not only on core-clock genes but also on the rhythmicity of genome expression. It would also be interesting to perform studies addressing the specific effect of IR on post-transcriptional (Crosby et al., 2019; Dang et al., 2016; Sinturel et al., 2017; Wang et al., 2018), translational (Atger et al., 2015; Jouffe et al., 2013; Mauvoisin et al., 2014; Sinturel et al., 2017), or post-translational events (Mauvoisin et al., 2014, 2017; Mauvoisin and Gachon, 2020).

Finally, it is well known that feeding is a dominant signal for the liver clock and the rhythmicity of gene expression (Damiola et al., 2000; Greenwell et al., 2019; Saini et al., 2013; Stokkan et al., 2001; Vollmers et al., 2009). Our work sheds light on the importance of intact hepatocyte IR for the oscillation of gene expression in response to feeding.

Diet-induced obesity (Kohsaka et al., 2007; Eckel-Mahan et al., 2013; Guan et al., 2018; Quagliarini et al., 2019) and time-restricted feeding (Saini et al., 2013; Stokkan et al., 2001; Vollmers et al., 2009) both influence the liver clock. Our findings support the hypothesis that such metabolic challenges that affect insulin signaling may reprogram the liver clock through

---

Figure 4. Hepatocyte-restricted deletion of the IR in adult mice disrupts reprogramming of rhythmic liver gene expression in response to DRF

(A) Cumulative number of rhythmic genes in the liver of IR$^{hep+/+}$ and IR$^{hep-/-}$ mice in function of minimal amplitude.

(B) Phase distribution of rhythmic genes in each condition. Euler diagrams show percentage of rhythmic genes in each genotype in regards to the feeding condition. Gray parts are genes are rhythmic in both genotypes.

(C) Histogram of the absolute time of phase shift. Euler diagram represents the percentage of shifting genes by genotype. Gray parts are genes found shifting in both genotypes.

(D) Number of genes classified in rhythmic models of interest as identified by dryR algorithm. A white square indicates no rhythm detected, and the identically filled square indicates shared rhythmic parameters (amplitude and phase). The number of genes per model is indicated.

(E) Heatmaps of normalized and averaged rhythmic mRNA levels (n = 3 per time point) around the clock (ZT0, ZT4, ZT8, ZT12, ZT16, ZT20) in the liver of IR$^{hep+/+}$ and IR$^{hep-/-}$ mice fed *ad libitum* (AdLib) or upon DRF. The height of the heatmaps in the left panel is proportional to the log2 number of genes. The colored curves on the top of the models schematize the phase distributions of genes. Groups with the same curve shape and the same color share the same rhythmic parameters. A black line indicates no rhythm detected. The right panel represents the phase distribution of the indicated models.

(F) Enrichment of genes found induced or repressed in mouse liver infused with insulin for 3 h (Batista et al., 2019b), food sensitive (Greenwell et al., 2019), Bmal1 sensitive (Atger et al., 2015), and with IR-bound promoters (Hancock et al., 2019).

(G) Top GO categories enriched by model. Hypergeometric tests performed over all models to assess the specificity of the enrichment.

(H) Functional enrichment around the clock. Enrichment of the indicated functional terms represented by the radial coordinate at the indicated time point.

changes in hepatocyte insulin sensitivity. Therefore, defective insulin signaling may contribute directly to the disruption of circadian homeostasis that occurs in diabetes and its complications. Conversely, time-restricted feeding is beneficial for metabolic health (Chaix et al., 2014, 2019; Hatori et al., 2012), and it is possible that the benefits of such nutritional intervention partly rely on insulin-dependent reprogramming of metabolism.

Limitations of the study

IR deletion has a potent effect on the liver and on metabolic homeostasis. Therefore, we cannot rule out the possibility that some of the changes in rhythmic gene expression reported here might not directly relate to altered insulin signaling. Moreover, we did not identify which specific pathway downstream of hepatic IR is involved in the control of rhythmic liver gene expression. Future work will aim at identifying this mechanism and exploring its pathophysiological relevance.

STAR★METHODS

Detailed methods are provided in the online version of this paper and include the following:

- KEY RESOURCES TABLE
- RESOURCE AVAILABILITY
  - Lead contact
  - Materials availability
  - Experimental model and subject details
  - Data and code availability
- METHOD DETAILS
  - Blood and tissue sampling in mice
  - Analysis of feeding behavior
  - Oral glucose tolerance test
  - Immunoblotting
  - Plasma analysis
  - ^{1}H-NMR based metabolomics
  - RNA extraction and RT-qPCR
  - Microarray
  - Microarray data analysis
- QUANTIFICATION AND STATISTICAL ANALYSIS

REFERENCES

Atger, F., Gobet, C., Marquis, J., Martin, E., Wang, J., Weger, B., Lefebvre, G., Descombes, P., Naef, F., and Gachon, F. (2015). Circadian and feeding rhythms differentially affect rhythmic mRNA transcription and translation in mouse liver. Proc. Natl. Acad. Sci. U S A *112*, E6579–E6588.

Aviram, R., Dandavate, V., Manella, G., Golik, M., and Asher, G. (2021). Ultradian rhythms of AKT phosphorylation and gene expression emerge in the absence of the circadian clock components Per1 and Per2. PLoS Biol. *19*, e3001492.

Bass, J., and Takahashi, J.S. (2010). Circadian integration of metabolism and energetics. Science *330*, 1349–1354.

Batista, T.M., Cederquist, C.T., and Kahn, C.R. (2019a). The insulin receptor goes nuclear. Cell Res. *29*, 509–511.

Batista, T.M., Garcia-Martin, R., Cai, W., Konishi, M., O'Neill, B.T., Sakaguchi, M., Kim, J.H., Jung, D.Y., Kim, J.K., and Kahn, C.R. (2019b). Multi-dimensional transcriptional remodeling by physiological insulin in vivo. Cell Rep. *26*, 3429–3443.e3.

Benjamini, Y., and Hochberg, Y. (1995). Controlling the false discovery rate: A practical and powerful approach to multiple testing. J. Royal Statistical Society, Series B (Methodological). *57 (1)*, 289–300.

Benjamini, Y., Krieger, A.M., and Yekutieli, D. (2006). Adaptive linear step-up procedures that control the false discovery rate. Biometrika *93 (3)*, 491–507.

Biddinger, S.B., Hernandez-Ono, A., Rask-Madsen, C., Haas, J.T., Alemán, J.O., Suzuki, R., Scapa, E.F., Agarwal, C., Carey, M.C., Stephanopoulos, G., et al. (2008). Hepatic insulin resistance is sufficient to produce dyslipidemia and susceptibility to atherosclerosis. Cell Metab. *7*, 125–134.

Bolstad, B.M., Irizarry, R.A., Astrand, M., and Speed, T.P. (2003). A comparison of normalization methods for high density oligonucleotide array data based on variance and bias. Bioinformatics *19*, 185–193.

Boucher, J., Macotela, Y., Bezy, O., Mori, M.A., Kriauciunas, K., and Kahn, C.R. (2010). A kinase-independent role for unoccupied insulin and IGF-1 receptors in the control of apoptosis. Sci. Signal *7*, ra87.

Brown, M.S., and Goldstein, J.L. (2008). Selective versus total insulin resistance: a pathogenic paradox. Cell Metab. *7*, 95–96.

Chaix, A., Zarrinpar, A., Miu, P., and Panda, S. (2014). Time-restricted feeding is a preventative and therapeutic intervention against diverse nutritional challenges. Cell Metab. *20*, 991–1005.

Chaix, A., Manoogian, E.N.C., Melkani, G.C., and Panda, S. (2019). Time-restricted eating to prevent and manage chronic metabolic diseases. Annu. Rev. Nutr. *39*, 291–315.

Crosby, P., Hamnett, R., Putker, M., Hoyle, N.P., Reed, M., Karam, C.J., Maywood, E.S., Stangherlin, A., Chesham, J.E., Hayter, E.A., et al. (2019). Insulin/IGF-1 drives PERIOD synthesis to entrain circadian rhythms with feeding time. Cell *177*, 896–909.

Damiola, F., Le Minh, N., Preitner, N., Kornmann, B., Fleury-Olela, F., and Schibler, U. (2000). Restricted feeding uncouples circadian oscillators in peripheral tissues from the central pacemaker in the suprachiasmatic nucleus. Genes Dev. *14*, 2950–2961.

Dang, F., Sun, X., Ma, X., Wu, R., Zhang, D., Chen, Y., Xu, Q., Wu, Y., and Liu, Y. (2016). Insulin post-transcriptionally modulates Bmal1 protein to affect the hepatic circadian clock. Nat. Commun. *31*, 12696.

Dong, X.C., Copps, K.D., Guo, S., Li, Y., Kollipara, R., DePinho, R.A., and White, M.F. (2008). Inactivation of hepatic Foxo1 by insulin signaling is required for adaptive nutrient homeostasis and endocrine growth regulation. Cell Metab. *8*, 65–76.

Droin, C., Kholtei, J.E., Bahar Halpern, K., Hurni, C., Rozenberg, M., Muvkadi, S., Itzkovitz, S., and Naef, F. (2021). Space-time logic of liver gene expression at sub-lobular scale. Nat. Metab. https://doi.org/10.1038/s42255-020-00323-1.

Eckel-Mahan, K.L., Patel, V.R., de Mateo, S., Orozco-Solis, R., Ceglia, N.J., Sahar, S., Dilag-Penilla, S.A., Dyar, K.A., Baldi, P., and Sassone-Corsi, P. (2013). Reprogramming of the circadian clock by nutritional challenge. Cell *155*, 1464–1478.

Edgar, R., Domrachev, M., and Lash, A.E. (2002). Gene expression omnibus: NCBI gene expression and hybridization array data repository. Nucleic Acids Res. *30*, 207–210.

Gentleman, R.C., Carey, V.J., Bates, D.M., Bolstad, B., Dettling, M., Dudoit, S., Ellis, B., Gautier, L., Ge, Y., Gentry, J., et al. (2004). Bioconductor: open software development for computational biology and bioinformatics. Genome Biol. *5*, R80.

Green, C.B., Takahashi, J.S., and Bass, J. (2008). The meter of metabolism. Cell *134*, 728–742.

Greenwell, B.J., Trott, A.J., Beytebiere, J.R., Pao, S., Bosley, A., Beach, E., Finegan, P., Hernandez, C., and Menet, J.S. (2019). Rhythmic food intake drives rhythmic gene expression more potently than the hepatic circadian clock in mice. Cell Rep. *27*, 649–657.e5.

Guan, D., and Lazar, M.A. (2021). Interconnections between circadian clocks and metabolism. J. Clin. Invest. *131*, e148278.

Guan, D., Xiong, Y., Borck, P.C., Jang, C., Doulias, P.T., Papazyan, R., Fang, B., Jiang, C., Zhang, Y., Briggs, E.R., et al. (2018). Diet-induced circadian enhancer remodeling synchronizes opposing hepatic lipid metabolic processes. Cell *174*, 831–842.e12.

Guan, D., Xiong, Y., Trinh, T.M., Xiao, Y., Hu, W., Jiang, C., Dierickx, P., Jang, C., Rabinowitz, J.D., and Lazar, M.A. (2020). The hepatocyte clock and feeding control chronophysiology of multiple liver cell types. Science *369*, 1388–1394.

Haas, J.T., Miao, J., Chanda, D., Wang, Y., Zhao, E., Haas, M.E., Hirschey, M., Vaitheesvaran, B., Farese, R.V., Jr., Kurland, I.J., et al. (2012). Hepatic insulin signaling is required for obesity-dependent expression of SREBP-1c mRNA but not for feeding-dependent expression. Cell Metab. *15*, 873–884.

Han, H., Cho, J.W., Lee, S., Yun, A., Kim, H., Bae, D., Yang, S., Kim, C.Y., Lee, M., Kim, E., et al. (2018). TRRUST v2: an expanded reference database of human and mouse transcriptional regulatory interactions. Nucleic Acids Res. *4;46*, D380–D386.

Hancock, M.L., Meyer, R.C., Mistry, M., Khetani, R.S., Wagschal, A., Shin, T., Ho Sui, S.J., Näär, A.M., and Flanagan, J.G. (2019). Insulin receptor associates with promoters genome-wide and regulates gene expression. Cell *177*, 722–736.e22.

Hatori, M., Vollmers, C., Zarrinpar, A., DiTacchio, L., Bushong, E.A., Gill, S., Leblanc, M., Chaix, A., Joens, M., Fitzpatrick, J.A., et al. (2012). Time-restricted feeding without reducing caloric intake prevents metabolic diseases in mice fed a high-fat diet. Cell Metab. *15*, 848–860.

Hegarty, B.D., Bobard, A., Hainault, I., Ferré, P., Bossard, P., and Foufelle, F. (2005). Distinct roles of insulin and liver X receptor in the induction and cleavage of sterol regulatory element-binding protein-1c. Proc. Natl. Acad. Sci. U S A *102*, 791–796.

Horton, J.D., Goldstein, J.L., and Brown, M.S. (2002). SREBPs: activators of the complete program of cholesterol and fatty acid synthesis in the liver. J. Clin. Invest. *109*, 1125–1131.

Jang, H., Lee, G.Y., Selby, C.P., Lee, G., Jeon, Y.G., Lee, J.H., Cheng, K.K., Titchenell, P., Birnbaum, M.J., Xu, A., et al. (2016). SREBP1c-CRY1 signalling represses hepatic glucose production by promoting FOXO1 degradation during refeeding. Nat. Commun. *7*, 12180.

Jouffe, C., Cretenet, G., Symul, L., Martin, E., Atger, F., Naef, F., and Gachon, F. (2013). The circadian clock coordinates ribosome biogenesis. PLoS Biol. *11*, e1001455.

Kohsaka, A., Laposky, A.D., Ramsey, K.M., Estrada, C., Joshu, C., Kobayashi, Y., Turek, F.W., and Bass, J. (2007). High-fat diet disrupts behavioral and molecular circadian rhythms in mice. Cell Metab. *6*, 414–421.

Koronowski, K.B., Kinouchi, K., Welz, P.S., Smith, J.G., Zinna, V.M., Shi, J., Samad, M., Chen, S., Magnan, C.N., Kinchen, J.M., et al. (2019). Defining the independence of the liver circadian clock. Cell *177*, 1448–1462.e14.

Kubota, N., Kubota, T., Kajiwara, E., Iwamura, T., Kumagai, H., Watanabe, T., Inoue, M., Takamoto, I., Sasako, T., Kumagai, K., et al. (2016). Differential hepatic distribution of insulin receptor substrates causes selective insulin resistance in diabetes and obesity. Nat. Commun. *7*, 12977.

Kuriyama, K., Sasahara, K., Kudo, T., and Shibata, S. (2004). Daily injection of insulin attenuated impairment of liver circadian clock oscillation in the streptozotocin-treated diabetic mouse. FEBS Lett. *572*, 206–210.

Li, S., Brown, M.S., and Goldstein, J.L. (2010). Bifurcation of insulin signaling pathway in rat liver: mTORC1 required for stimulation of lipogenesis, but not inhibition of gluconeogenesis. Proc. Natl. Acad. Sci. U S A *107*, 3441–3446.

Matsumoto, M., PocaiP, A., Rossetti, L., Depinho, R.A., and Accili, D. (2007). Impaired regulation of hepatic glucose production in mice lacking the forkhead transcription factor Foxo1 in liver. Cell Metab. *6*, 208–216.

Mauvoisin, D., and Gachon, F. (2020). Proteomics in circadian biology. J. Mol. Biol. *432*, 3565–3577.

Mauvoisin, D., Wang, J., Jouffe, C., Martin, E., Atger, F., Waridel, P., Quadroni, M., Gachon, F., and Naef, F. (2014). Circadian clock-dependent and -independent rhythmic proteomes implement distinct diurnal functions in mouse liver. Proc. Natl. Acad. Sci. U S A *111*, 167–172.

Mauvoisin, D., Atger, F., Dayon, L., Núñez Galindo, A., Wang, J., Martin, E., Da Silva, L., Montoliu, I., Collino, S., Martin, F.P., et al. (2017). Circadian and feeding rhythms orchestrate the diurnal liver acetylome. Cell Rep. *20*, 1729–1743.

Michael, M.D., Kulkarni, R.N., Postic, C., Previs, S.F., Shulman, G.I., Magnuson, M.A., and Kahn, C.R. (2000). Loss of insulin signaling in hepatocytes leads to severe insulin resistance and progressive hepatic dysfunction. Mol. Cell *6*, 87–97.

Mohawk, J.A., Green, C.B., and Takahashi, J.S. (2012). Central and peripheral circadian clocks in mammals. Annu. Rev. Neurosciences *35*, 445–462.

Nagao, H., Cai, W., Wewer Albrechtsen, N.J., Steger, M., Batista, T.M., Pan, H., Dreyfuss, J.M., Mann, M., and Kahn, C.R. (2021). Distinct signaling by insulin and IGF-1 receptors and their extra- and intracellular domains. Proc. Natl. Acad. Sci. U S A *118*, e2019474118.

Nemazanyy, I., Montagnac, G., Russell, R.C., Morzyglod, L., Burnol, A.F., Guan, K.L., Pende, M., and Panasyuk, G. (2015). Class III PI3K regulates organismal glucose homeostasis by providing negative feedback on hepatic insulin signalling. Nat. Commun. *6*, 8283.

O'Sullivan, I., Zhang, W., Wasserman, D.H., Liew, C.W., Liu, J., Paik, J., DePinho, R.A., Stolz, D.B., Kahn, C.R., Schwartz, M.W., and Unterman, T.G.

(2015). FoxO1 integrates direct and indirect effects of insulin on hepatic glucose production and glucose utilization. Nat. Commun. *6*, 7079.

Pagès, H., Carlson, M., Falcon, S., and Li, N. (2021). AnnotationDbi: Manipulation of SQLite-based annotations in Bioconductor. R package version 1.54.1.

Panda, S. (2016). Circadian physiology of metabolism. Science *354*, 1008–1015.

Perelis, M., Ramsey, K.M., Marcheva, B., and Bass, J. (2016). Circadian transcription from beta cell function to diabetes pathophysiology. J. Biol. Rhythms *31*, 323–336.

Quagliarini, F., Mir, A.A., Balazs, K., Wierer, M., Dyar, K.A., Jouffe, C., Makris, K., Hawe, J., Heinig, M., Filipp, F.V., et al. (2019). Cistromic reprogramming of the diurnal glucocorticoid hormone response by high-fat diet. Mol. Cell *76*, 531–545.e5.

Régnier, M., Polizzi, A., Smati, S., Lukowicz, C., Fougerat, A., Lippi, Y., Fouché, E., Lasserre, F., Naylies, C., Bétoulières, C., et al. (2020). Hepatocyte-specific deletion of Pparα promotes NAFLD in the context of obesity. Sci. Rep. *10*, 6489.

Rijo-Ferreira, F., and Takahashi, J.S. (2019). Genomics of circadian rhythms in health and disease. Genome Med. *11*, 82.

Saini, C., Liani, A., Curie, T., Gos, P., Kreppel, F., Emmenegger, Y., Bonacina, L., Wolf, J.P., Poget, Y.A., Franken, P., and Schibler, U. (2013). Real-time recording of circadian liver gene expression in freely moving mice reveals the phase-setting behavior of hepatocyte clocks. Genes Dev. *27*, 1526–1536.

Sato, M., Murakami, M., Node, K., Matsumura, R., and Akashi, M. (2014). The role of the endocrine system in feeding-induced tissue-specific circadian entrainment. Cell Rep. *8*, 393–401.

Sinturel, F., Gerber, A., Mauvoisin, D., Wang, J., Gatfield, D., Stubblefield, J.J., Green, C.B., Gachon, F., and Schibler, U. (2017). Diurnal oscillations in liver mass and cell size accompany ribosome assembly cycles. Cell *169*, 651–663.

Smati, S., Régnier, M., Fougeray, T., Polizzi, A., Fougerat, A., Lasserre, F., Lukowicz, C., Tramunt, B., Guillaume, M., Burnol, A.F., et al. (2020). Regulation of hepatokine gene expression in response to fasting and feeding: influence of PPAR-α and insulin-dependent signalling in hepatocytes. Diabetes Metab. *46*, 129–136.

Smyth, G.K. (2004). Linear models and empirical bayes methods for assessing differential expression in microarray experiments. Stat. Appl. Genet. Mol. Biol. *3*, Article3.

Stokkan, K.A., Yamazaki, S., Tei, H., Sakaki, Y., and Menaker, M. (2001). Entrainment of the circadian clock in the liver by feeding. Science *291*, 490–493.

Takahashi, J.S. (2017). Transcriptional architecture of the mammalian circadian clock. Nat. Rev. Genet. *18*, 164–179.

Takahashi, J.S., Hong, H.K., Ko, C.H., and McDearmon, E.L. (2008). The genetics of mammalian circadian order and disorder: implications for physiology and disease. Nat. Rev. Genet. *9*, 764–775.

Titchenell, P.M., Lazar, M.A., and Birnbaum, M.J. (2017). Unraveling the regulation of hepatic metabolism by insulin. Trends Endocrinol. Metab. *28*, 497–505.

Vollmers, C., Gill, S., DiTacchio, L., Pulivarthy, S.R., Le, H.D., and Panda, S. (2009). Time of feeding and the intrinsic circadian clock drive rhythms in hepatic gene expression. Proc. Natl. Acad. Sci. U S A *106*, 21453–21458.

Wang, J., Symul, L., Yeung, J., Gobet, C., Sobel, J., Lück, S., Westermark, P.O., Molina, N., and Naef, F. (2018). Circadian clock-dependent and -independent posttranscriptional regulation underlies temporal mRNA accumulation in mouse liver. Proc. Natl. Acad. Sci. U S A *115*, E1916–E1925.

Weger, B.D., Gobet, C., David, F.P.A., Atger, F., Martin, E., Phillips, N.E., Charpagne, A., Weger, M., Naef, F., and Gachon, F. (2021). Systematic analysis of differential rhythmic liver gene expression mediated by the circadian clock and feeding rhythms. Proc. Natl. Acad. Sci. U S A *118*, e2015803118.

Weger, M., Weger, B.D., and Gachon, F. (2022). The mechanisms and physiological consequences of diurnal hepatic cell size. Cell Physiol Biochem. *56*, 1–11.

Yamajuku, D., Inagaki, T., Haruma, T., Okubo, S., Kataoka, Y., Kobayashi, S., Ikegami, K., Laurent, T., Kojima, T., Noutomi, K., et al. (2012). Real-time monitoring in three-dimensional hepatocytes reveals that insulin acts as a synchronizer for liver clock. Sci. Rep. *2*, 439.

STAR★METHODS

KEY RESOURCES TABLE

REAGENT or RESOURCE	SOURCE	IDENTIFIER
Antibodies		
Rabbit-anti-phospho-AKT Ser473	Cell Signaling Technology	Cat #4058; RRID:AB_331168
Rabbit-anti-AKT	Cell Signaling Technology	Cat #9272; RRID:AB_329827
Mouse-anti-Insulin Receptor β	Santa Cruz Biotechnology	Cat sc-57342; RRID:AB_784102
Rabbit-anti-β-Actin	Cell Signaling Technology	Cat #4970; RRID:AB_2223172
Goat anti-Rabbit IgG secondary	Cell Signaling Technology	Cat #7074s; RRID:AB_2099233
Horse anti-Mouse IgG secondary	Cell Signaling Technology	Cat #7076s; RRID:AB_330924
Chemicals, peptides and recombinant proteins		
Tamoxifen Free Base	MP Biomedicals	Cat #156738
D-(+)-Glucose	Sigma Aldrich	Cat #G7021
NaCl	Sigma Aldrich	Cat #S9888
Sodium deoxycholate	Sigma Aldrich	Cat #D6750
EDTA	Sigma Aldrich	Cat #03690
PMSF	Roche	Cat #10 837,091 001
Sodium orthovanadate	Sigma Aldrich	Cat #S6508
NP-40	Sigma Aldrich	Cat #56741
Aprotinin	Sigma	Cat #A1153
Leupeptin	Sigma	Cat #L2884
Tris-HCL	Euromedex	Cat #EU0011
Clarity ECL	Bio-Rad	Cat #170-5060
SYBR Green	Applied Biosystems	Cat #4367659
TRIzol Reagent	Invitrogen	Cat #TR118
Critical commercial assays		
Sureprint G3 Mouse G v2 microarrays	Agilent Technologies	N/A
Hot star Taq DNA polymerase	Quiagen	Cat #203605
High capacity cDNA RT kit	ThermoFisher	Cat #4368813
BCA Protein Assay Kit	ThermoFisher	Cat #23227
Deposited data		
Raw and processed data (Microarray);	GEO (http://www.ncbi.nlm.nih.gov/geo/)	GSE165154
Raw and processed data (Microarray)	GEO (http://www.ncbi.nlm.nih.gov/geo/)	GSE165155
Raw and processed data (Microarray)	GEO (http://www.ncbi.nlm.nih.gov/geo/)	GSE165156
Experimental models: Organisms/strains		
Mouse: C57/Bl6J-$IR^{hep+/+}$	Namazanyy et al. (2015); Smati et al. (2020)	N/A
Mouse: C57/Bl6J-$IR^{hep-/-}$	Namazanyy et al. (2015); Smati et al. (2020)	N/A
Oligonucleotides		
Primers for RT-qPCR analysis, see Table S1	This paper	N/A
Software and algorithms		
LinRegPCR	Jan Rujiter	http://LinRegPCR.nl
R	N/A	https://www.r-project.org
DryR package	Weger et al. (2021)	https://www.r-project.org
GraphPad Prism	Prism 7	https://www.graphpad.com
BioDAQ Data Viewer	Research diet	N/A
Others		
Nitrocellulose Blotting Membrane	Bio-Rad	Cat #620112
Standard Rodent diet SAFE A04	Safe	U8220G10R
AccuCheck Performa glucometer	Roche Diagnostics	N/A
EDTA coated tubes	Bd Microtainer	K2E tubes

RESOURCE AVAILABILITY

Lead contact

Further information and requests for resources and reagents should be directed to and will be fulfilled upon reasonable request by the lead contact, Hervé Guillou (herve.guillou@inrae.fr).

Materials availability

All reagents generated in this study are available from the lead contact without restriction.

Experimental model and subject details

In vivo studies were performed in accordance with European guidelines for the use and care of laboratory animals, and approved by an independent Ethics Committee (C3155513; APAFiS #14112–2018031611107639 and APAFiS #16702-2018090717531086v2).

To generate tamoxifen-inducible hepatocyte-specific IR knockout mouse line (IR$^{hep-/-}$) and their control (IR$^{hep+/+}$), animals carrying *LoxP* sites flanking the fourth exon of the IR gene (IRlox/lox stock number: 006,955; Jackson Laboratory, Bar Harbor, ME, USA) were intercrossed with C57BL/6J mice, which specifically express Cre recombinase in the liver under the transthyretin promoter (TTR-CreTam mice), as previously described (Nemazanyy et al., 2015; Smati et al., 2020).

At the age of 8 weeks, males IR$^{hep-/-}$ (IR$^{floxed/floxed/TTR-CreTam+/+}$) and IR$^{hep+/+}$ (IR$^{floxed/floxed/TTR-CreTam-/-}$) mice received tamoxifen (Tamoxifen Free Base, MP Biomedicals) by intraperitoneal injection (1.5 mg/kg) during three consecutive days, in order to induce deletion of hepatocyte Insulin receptor.

All the mice used were males. *Ad libitum* experiments were performed in 12 week-old mice. Daytime Restricted Feeding experiments started two weeks after the last tamoxifen injection and mice were killed when 12 week-old.

The IR deletion was confirmed in IR$^{hep-/-}$ mice with PCR and HotStar Taq DNA Polymerase (5 U/μl, Qiagen) using the following primers: IR-forward: 5′-GATGTGCACCCCATGTCTG-3′; IR-reverse: 5′-CTGAATAGCTGAGACCACAG-3′ and IRdelta: 5′-GGGTAGGAAACAGGATGG-3′. The amplification conditions were as follows: 95°C for 5 min, followed by 35 cycles of 94°C for 30 s, 65°C for 30 s, and 72°C for 45 s, and a final cycle of 72°C for 7 min. This reaction produced 300-bp, which represented the IR sequence with the floxed allele. The TTR-CreTam allele was detected by PCR using the following primers: forward: 5′-CCTGGAAAATGCTTCTGTCCG-3′ and reverse: 5′-CAGGGTGTTATAAGCAATCCC-3′.

All mice were fed a standard rodent diet (Safe 04 U8220G10R), and housed under controlled temperature (21–23°C) and light (12-h light/12-h dark) conditions: lights were turned on at Zeitgeber time (ZT) 0 and turned off at ZT12. For DRF, mice were adapted during 2 weeks to eat during the light period, and food was removed at the beginning of the dark period, as previously described (Damiola et al., 2000).

Data and code availability

- Gene expression profiles are deposited in the Gene Expression Omnibus (GEO) database under the accession number GSE165154; GSE165155; GSE165156.
- This paper does not report original code.
- Any additional information required regarding this paper is available from the lead contact upon request.

METHOD DETAILS

Blood and tissue sampling in mice

Prior to sacrifice, blood was collected into EDTA coated tubes (BD Microtainer, K2E tubes) from the submandibular vein. All mice were killed in a fed state (unless stated otherwise). Plasma was collected by centrifugation (1,500 × g, 15min, 4°C) and stored at −80°C. Following killing by cervical dissociation, organs were removed, weighted, dissected and used for snap frozen in liquid nitrogen and stored at −80°C.

Analysis of feeding behavior

Mice were acclimatized for 3 days to single housing and feeding through the food hopper (BioDAQ System; Research Diets, USA). Cages contained enrichment and bedding material. Water was given *ad libitum* from regular bottles placed on the top of the cage. Data were collected continuously and were analyzed using the BioDAQ DataViewer software. For analysis, minimum food amount was filtered at 0.01 g. Statistics were done on raw data using Prism software (v5.0; GraphPad). For illustration, data of each mouse were oversampled by extrapolation to define a value/second, averaged for each genotype, and smoothed with a Savitzky-Golay filter, using Matlab software.

Oral glucose tolerance test

OGTT was performed one month after the last tamoxifen injection. Mice were fasted for 6 h and received an oral (2g/kg body weight) glucose load (G7021, Sigma Aldrich). Blood glucose was measured at the tail vein using an AccuCheck Performa glucometer (Roche Diagnostics) at −15, 0, 15, 30, 45, 60, 90, and 120 min.

Immunoblotting

Frozen liver, white and brown adipose tissue samples, were homogenized in a lysis buffer [50 mM Tris-HCl (pH 7,4), 150 mM sodium chloride (NaCl), 1% NP-40, 0.25% sodium deoxycholate, 0.1% sodium dodecyl sulfate (SDS), 2 mM ethylenediaminetetraacetic acid (EDTA) and 1 mM phenylmethylsulfonyl fluoride (PMSF)] supplemented with 2 μg/mL aprotinin, 5 μg/mL leupeptin and 1 mM sodium orthovanadate for 30 min at 4°C. Samples were then centrifuged at 13,000 rpm for 30 min at 4°C. Supernatants were collected and the protein concentration in each lysate was measured using BC Assay Protein Quantification Kits (Interchim, Montluçon, France). Proteins (20–30 μg) were separated by SDS-PAGE (polyacrylamide gel electrophoresis) and transferred onto nitrocellulose membranes, which were first incubated overnight at 4°C with primary antibodies against Insulin receptor β (sc-57342, Santa Cruz Biotechnology, Santa Cruz, CA, USA), pSer473AKT (#4058, Cell Signaling Technology, Beverly, MA, USA), total AKT (#9272, Cell Signaling Technology, Beverly, MA, USA) and β-actin (#4970, Cell Signaling Technology, Beverly, MA, USA), and then with horseradish peroxidase-conjugated secondary antibodies (anti-mouse for Insulin receptor β detection and anti-rabbit for all others) for 1 h at room temperature. Immunoreactive proteins were detected with Clarity Western ECL blotting substrate (Bio-Rad Laboratories, Hercules, CA, USA) according to the manufacturer's instructions, and signals were acquired using the Chemidoc Touch Imaging System (Bio-Rad).

Plasma analysis

Plasma samples were assessed for free fatty acids, triglycerides, total cholesterol and low-density lipoprotein (LDL) cholesterol levels, using a Cobas Mira Plus biochemical analyzer (Roche Diagnostics, Indianapolis, IN, USA), at the ANEXPLO/Genotoul Zootechnics Core Facilities in Toulouse. Plasma Insulin and Glucagon concentration was assessed using Insulin mouse serum Assay HTRF Kit (Cisbio) and Glucagon mouse serum Assay HTRF kit (Cisbio), at the WE-MET in Toulouse. Blood glucose was measured with an Accu-Chek Go glucometer (Roche Diagnostics).

^{1}H-NMR based metabolomics

Liver polar extracts were prepared for NMR analysis as described previously (Regnier et al., 2020). All ^{1}H-NMR spectra were obtained on a Bruker DRX-600-Avance NMR spectrometer (Bruker, Wissembourg, France) using the AXIOM metabolomics platform (MetaToul) operating at 600.13 MHz for 1H resonance frequency using an inverse detection 5-mm 1H-13C-15N cryoprobe attached to a cryoplatform (the preamplifier cooling unit).

RNA extraction and RT-qPCR

Total cellular RNA was extracted using TRI Reagent (Molecular Research Center, Inc., Cincinnati, OH, USA). Total RNA samples (2 μg) were reverse-transcribed using High Capacity cDNA Reverse Transcription Kits (Thermo Fisher Scientific, Waltham, MA, USA) for real-time quantitative polymerase chain reaction (qPCR) analyses; the primers used for the SYBR Green assays are listed in Table S3. Amplifications were performed using a Stratagene Mx3005P system (Agilent Technologies, Santa Clara, CA, USA). The qPCR data were normalized to the level of *Psmb6* (proteasome 20S subunit beta 6) transcripts, and analyzed using LinRegPCR.v2015.3 to get the starting concentration (N0) which is calculated as follow: N0 = threshold/(Eff meanCq) with Eff mean: mean PCR efficiency and Cq: quantification cycle.

Microarray

Gene expression profiles were obtained at the GeT-TRiX facility (GenoToul, Genopole Toulouse Midi-Pyrénées) using Agilent Sureprint G3 Mouse GE v2 microarrays (8 × 60K, design 074,809) following the manufacturer's instructions.

For each sample, Cyanine-3 (Cy3) labeled cRNA was prepared from 200 ng of total RNA using the One-Color Quick Amp Labeling kit (Agilent) according to the manufacturer's instructions, followed by Agencourt RNAClean XP (Agencourt Bioscience Corporation, Beverly, Massachusetts). Dye incorporation and cRNA yield were checked using a Dropsense 96 UV/VIS droplet reader (Trinean, Belgium). A total of 600 ng of Cy3-labelled cRNA was hybridized on the microarray slides following the manufacturer's instructions. Immediately after washing, the slides were scanned on an Agilent G2505C Microarray Scanner using Agilent Scan Control A.8.5.1 software and the fluorescence signal extracted using Agilent Feature Extraction software v10.10.1.1 with default parameters. Microarray data and experimental details are available in NCBI's Gene Expression Omnibus (Edgar et al., 2002) and are accessible through GEO Series accession numbers GSE165154 and GSE165155.

Microarray data analysis

Microarray data were analyzed using R (R Development Core Team, 2008) and Bioconductor packages: www.bioconductor.org, v 3.0 (Gentleman et al., 2004), as described in GEO accession GSE165156. Raw data (median signal intensity) were filtered, log2 transformed, corrected for batch effects (microarray washing bath and labeling serials) and normalized using quantile method (Bolstad, et al., 2003).

A model was fitted using the limma lmFit function (Smyth, 2004). Pairwise comparisons between biological conditions were applied using specific contrasts to extract genotype, Time and Genotype: Time interaction effects. A correction for multiple testing was applied using the Benjamini-Hochberg procedure (BH, Benjamini and Hochberg, 1995; Benjamini et al., 2006) to control the False Discovery Rate (FDR). Probes with FDR ≤0.05 were considered to be differentially expressed between conditions.

Hierarchical clustering was applied to the samples and the differentially expressed probes using the 1-Pearson correlation coefficient as distance and Ward's criterion for agglomeration. The clustering results are illustrated as a heatmap of expression signals.

To assess rhythmicity and mean differences of gene expression in gene expression analysis we used the drylm function of the dryR package built by Weger et al. (2021): dryR: Differential RhythmicitY analysis; R package version 1.0.0., a model selection framework based on generalized linear models (GLMs).

QUANTIFICATION AND STATISTICAL ANALYSIS

Statistical analysis were performed using GraphPad Prism version 8 for Mac OS X (GraphPad Software, San Diego, CA) except for microarray data analysis that was performed as described in the method details section (Microarray data analysis).

Values are presented as mean ± sem. The n number refers to the number of animals. Details regarding the specific statistical tests used are provided in the figure legends. When appropriate, multiple t test was performed to determine statistical differences between two groups followed by appropriate correction (Benjamini et al., 2006). For experiments with more than 2 factors, two-way ANOVA was performed to assess differences between means followed by appropriate post-hoc tests (Sidak's multiple comparisons test) to determine statistical significance between groups.